Analysis of Stress Transfer in Two-Phase Polymer Systems Using Synchrotron Microfocus X-ray Diffraction

Robert J. Young,*,† Stephen J. Eichhorn,† Yat-Tarng Shyng,† Christian Riekel,‡ and Richard J. Davies‡

Manchester Materials Science Centre, UMIST/University of Manchester, Grosvenor Street, Manchester, M1 7HS, UK, and European Synchrotron Radiation Facility, B.P. 220, F-38043, Grenoble Cedex, France

Received July 23, 2004; Revised Manuscript Received September 23, 2004

ABSTRACT: Microfocus X-ray diffraction has been used to analyze interfacial stress transfer in two-phase polymer systems consisting of a highly oriented polymer fiber in an isotropic resin matrix. Synchrotron radiation has been used to obtain high-quality X-ray diffraction patterns from single poly(*p*-phenylene benzobisoxazole) (PBO) and poly(*p*-phenylene terephthalamide) (PPTA) fibers in these model two-phase systems. Two different specimen geometries were studied: a fully embedded fiber composite and a microdroplet specimen. A procedure is demonstrated whereby well-defined diffraction patterns can be obtained, using a 5 μm diameter X-ray beam, from individual 12 μm diameter polymer fibers in over 1 mm thickness of resin by subtracting the scattering of the resin matrix from that of the fiber and matrix to obtain a diffraction pattern of the fiber only. Shifts of meridional diffraction peaks of the fibers were determined as a function of stress and were converted into crystal strain. The fiber stress was then determined from calibrations obtained from previous X-ray diffraction studies of fiber deformation. The point-to-point variation of fiber stress was mapped along the fibers in the specimens, and a force-balance approach was used to determine the shear stress at the fiber−matrix interface. This present study was concerned only with an optically transparent polymer matrix, but the possible extension of the technique to opaque matrices and other multiphase polymer systems is discussed.

Introduction

This report is concerned with a new technique that can be employed to monitor stress in one of the phases in a multiphase polymer system through the use of synchrotron microfocus X-ray diffraction. A specific example is given of the local measurement of stress in high-performance polymer fibers in an epoxy resin matrix. Multiphase polymer systems such as fiber-reinforced composites are being used increasingly in structural engineering applications, but their performance is limited by the strength of the fiber−matrix interface among other factors such as fiber strength and aspect ratio. Synchrotron radiation has been proven to be a powerful tool for studying the structure and deformation of high-performance polymer fibers[1−3] such as PBO and PPTA[4−6] (Figure 1). It is well-known that their so-called "rigid-rod" structures are able to sustain a high tensile load for a relatively low elongation. Furthermore, the well-packed and highly crystalline structures of these fibers give strong and well-defined X-ray diffraction patterns.[1−3] These diffraction patterns can be obtained from individual PBO and PTTA polymer fibers using synchrotron radiation, without significant radiation damage, using exposure times of only a few seconds.

The origin of the poly(*p*-phenylene benzobisoxazole) (PBO) fiber can be traced back to the late 1960s when the U.S. Air Force was researching for a new fiber material with good mechanical properties and heat resistance.[5] Because of the rigid-rod form of its molecular structure as illustrated in Figure 1a, the PBO fiber possesses outstanding mechanical properties, long-term stability, and excellent tolerance of high temperature. Currently, it is commercialized by Toyobo[6] under the trade name Zylon.

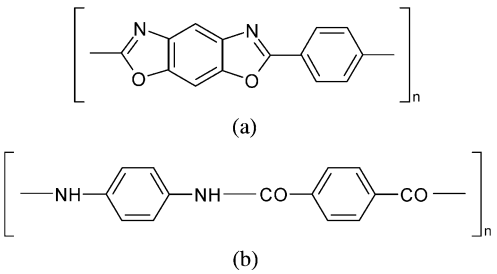

Figure 1. Molecular structures of (a) PBO and (b) PPTA aramid fibers.

The poly(*p*-phenylene terephthalamide) (PPTA) fiber was first developed by the Du Pont Co. in 1965 and then commercialized in 1972 as Kevlar. The polymeric repeat unit of PPTA fibers is shown in Figure 1b. Initially, the Kevlar fiber was designed as a composite reinforcement material but has since been widely applied to many applications.[4] More recently, Teijin has commercialized a PPTA fiber under the trade name of Twaron.

The interfacial strain or stress distributions of a single-fiber model composite have been studied extensively, and the most common technique applied in this field has been Raman spectroscopy.[7−9] The stress distribution along an individual fiber can be determined from the shift of Raman bands by scanning the laser beam along the fiber inside the resin. The shear stress at the interface can be calculated by determining the rate of change of fiber stress with respect to position along the fiber.

† UMIST/University of Manchester.
‡ European Synchrotron Radiation Facility.
* Corresponding author: Tel +44-161-200-3551; Fax +44-161-200-8877; e-mail robert.young@umist.ac.uk.

10.1021/ma048484x CCC: $27.50
Published on Web 11/18/2004

However, the Raman spectroscopy approach has several limitations. First, it is essential that the matrix is either transparent, or at least partially transparent, to allow the laser beam to penetrate the resin. The use of opaque matrices, such as the widely used engineering polymers, PP (polypropylene) and PEEK (polyetheretherketone), is therefore precluded. Second, a number of fiber−matrix combinations, the Raman bands from the matrix are at a similar wavenumber to those of the fiber, and it is difficult to deconvolute them.

In this study, the deformation of different geometries of model two-phase polymer systems, consisting of a highly oriented polymer fiber in an epoxy resin, has been examined on the microfocus beamline ID13 of the ESRF (European Synchrotron Radiation Facility). The stress distributions along individual polymer fibers have been mapped using a 5 μm diameter X-ray beam both outside and inside the resin matrix. Synchtrotron X-ray diffraction, although useful compared to Raman spectroscopy in terms of the ability to probe fiber stresses in opaque matrix composite systems, does pose additional problems such as radiation damage, and these will be discussed with a view to further development. The use of synchrotron X-ray diffraction for the analysis of deformation micromechanics is explained, with particular emphasis on a unique droplet geometry, but more general applications of the technique are also discussed. In particular, it is thought that this technique could be used to map strains in general two-phase polymeric systems. Specific examples of this would be all-polymer composites where oriented and nonoriented phases exist and also in copolymer blends and at biopolymer/mineral interfaces.

Experimental Methods

Materials. The PBO and PPTA fibers investigated in this study were supplied by Toyobo, Japan, and Teijin, Japan, respectively. Both fiber types are produced commercially under the trade names of Zylon (PBO) and Twaron (PPTA). A Philips 525M scanning electron microscope (SEM) was used to determine fiber diameters. At least 20 fibers of each type were selected randomly and then examined at three different magnification levels. Average diameters and standard deviations were calculated for each fiber type with accuracy ensured through calibration using a standard grid. The average values of fiber diameter and their standard deviations were found to be 11.2 ± 0.7 and 12.1 ± 0.5 μm for the PBO and PPTA fibers, respectively.

Single-Fiber Embedded Model Composites. They were prepared using a rectangular mold and the matrix material employed was a cold-curing two-part epoxy resin supplied by Ciba Geigy, UK. It consisted of 100 parts by weight of butane-1,4-diol diglycidyl ether resin (LY5052) and 38 parts by weight of isophorone diamine hardener (HY5052). The mold was filled with resin, and a single straight PBO fiber, cut to a length of about 10 mm using ceramic scissors, was inserted through the top surface of the resin to form the model two-phase polymer system. The epoxy was then cured at room temperature for 7 days before being cut into strips and shaped into dumbbell test specimens ~2 mm thick.

Microdroplet Specimens. The fibers were mounted in a paper frame with a 50 mm gauge length. A single straight PPTA filament was cut and secured to the paper frame by cyanoacrylate adhesive in order to give good adhesion and prevent the slippage of fiber during the test. Droplets of epoxy resin (again 100 parts by weight of LY5052 and 38 parts by weight of HY5052 cured at room temperature for 7 days) up to 500 μm diameter were then applied to the middle of the filament using fine tweezers. A more detailed description of a similar procedure has previously been reported elsewhere.[10] Both sides of the paper frame were burned or cut away before testing.

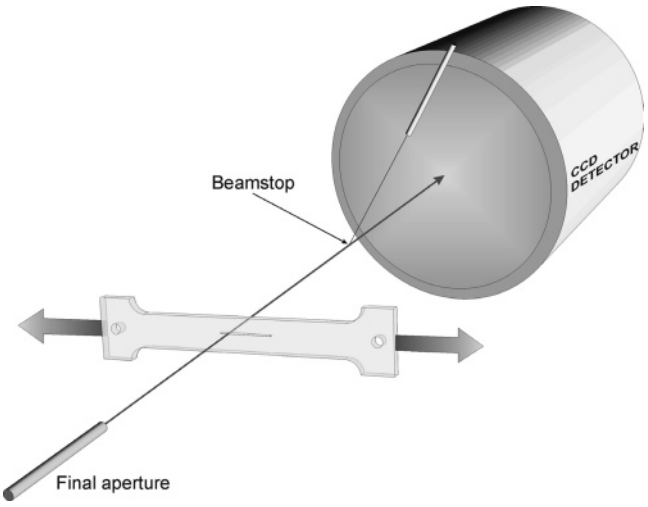

Figure 2. Schematic diagram of the experimental setup for the single-fiber embedded composite.

Microfocus X-ray Diffraction. The X-ray microdiffraction experiments were conducted at the European Synchrotron Radiation Facility (ESRF), Grenoble, France, on beamline ID13. The beamline was configured with a pair of Kirkpatrick−Baez (KB)-type mirrors. The focused beam was then collimated using a piezo-based block collimation system and passed through a final aperture incorporating an ionization chamber that provides a value for the beam intensity for each exposure which enables subsequent normalization. The collimation system provided an on-sample beam spot size of approximately 5 μm with a radiation wavelength of 0.095 nm. A charge-coupled device (CCD) detector with an average pixel size of 257.79 μm^2 was used to capture diffraction patterns. All patterns were obtained using an exposure time of up to 10 s, and the specimen-to-detector distance was calculated from the diffraction pattern of an Al_2O_3 calibration sample.

The experimental setup is shown schematically in Figure 2 for the single-fiber embedded composite. The specimen was mounted on a Minimat tensile straining rig and deformed by moving the crosshead manually. The specimen and straining rig were scanned though the beam in 20 μm steps at each loading level.

Calculation of Fiber Crystal Strain and Crystal Modulus. Analysis of the diffraction data was performed using a combination of the FIT2D software application[11,12] and batch-processing software. Radial profiles were first generated which allowed the positions of the fiber meridional reflections to be determined. This enabled the subsequent calculation of lattice spacings in the fiber axis direction (commonly referred to as *c*-spacing) using one-dimensional diffraction grating theory according to[13]

$$c = \frac{n\lambda}{\sin\left[\tan^{-1}\left(\frac{h}{r}\right)\right]} \tag{1}$$

where n is the order of diffraction, λ is the X-ray wavelength, r is the sample-to-detector distance, and h is the distance of the reflection from beam center. A more detailed description of a similar analysis procedure has previously been reported elsewhere.[1] The crystal strain (ϵ_c) may then be calculated as the change in lattice spacing during sample deformation using

$$\epsilon_c = \frac{c_\sigma - c_0}{c_0} \tag{2}$$

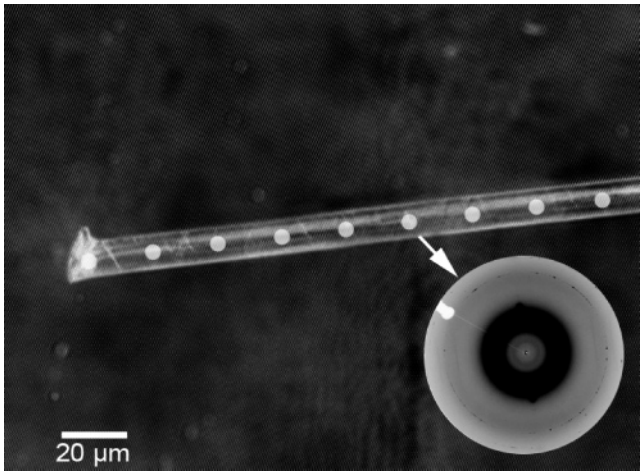

Figure 3. Optical micrograph of the single fiber model PBO/epoxy composite specimen taken in the vicinity of the fiber end showing a typical diffraction pattern obtained from the fiber and resin.

where c_0 is the c-spacing determined from an undeformed fiber and c_σ is the c-spacing determined from the sample at a stress level of σ. The calculation of crystal modulus (E_c) may also be performed using

$$E_c = \frac{\sigma}{\epsilon_c} \tag{3}$$

For such calculations it is necessary to assume that stresses acting upon crystallite domains within the fibers are the same as macroscopic fiber stress and that the crystal behaves linear elastically.

Results and Discussion

Single-Fiber Embedded Composite. Figure 3 shows an optical micrograph, obtained using the beamline microscope, of a model composite consisting of a single PBO fiber in the epoxy matrix. It can be seen that the fiber was aligned at about 10° to the tensile axis (horizontal). The micrograph shows the cut end of the fiber and the series of 5 μm diameter circles represent the positions where the diffraction patterns were obtained at 20 μm intervals along the fiber. A typical diffraction pattern is also shown superimposed on the micrograph. It can be seen that the cutting process (using the ceramic scissors) caused some damage to the fiber end, and a number of kink bands[14] at an angle of about 55° to the fiber axis can also be seen in this region.

The diffraction pattern shown in Figure 3 has contributions from both the PBO fiber and epoxy matrix. The FIT2D program procedure was used to subtract the diffraction pattern obtained from the matrix region adjacent to the fiber to give a diffraction pattern of the fiber only. There was no need to account for air scattering since it contributed similarly to both diffraction patterns. It was necessary to use the ionization chamber intensity values to correct for intensity fluctuations of the incoming beam, and the subtraction procedure is shown schematically in Figure 4. It was found to be very similar to that obtained for a single PBO fiber in air[1] with no evidence of radiation damage. The orientation of the diffraction pattern is consistent with the fiber being orientated at an angle of about 10° to the horizontal.

The procedure shown in Figure 4 is remarkable in that it demonstrates that it is possible to obtain a well-defined X-ray diffraction pattern from a 5 μm region of a single 12 μm diameter fiber of PBO inside a block of epoxy resin over 1 mm thick. The fiber therefore only contributes to less than 1% of the material in the X-ray beam. There are a number of reasons that this is possible: (i) The diffraction pattern from the fiber is very well-defined, and for a similar thickness of material, the diffraction spots are considerably more intense than the diffuse rings of the epoxy pattern. (ii) The CCD camera employed has a large dynamic range and captures the diffraction patterns very accurately with negligible noise. (iii) The FIT2D program[12] enables corrections to be made for fluctuations in X-ray beam intensity and accurate manipulation of the X-ray diffraction patterns.

The point-to-point variation of axial fiber stress was determined from the shift of the meridional reflections[1] of the PBO fiber relative to an undeformed fiber in air and eq 2. This was undertaken for the unloaded specimen and the specimen at three different arbitrary loading levels as shown in Figure 5a. A prior investigation[1,3] upon the deformation of the individual PBO fibers showed that a crystal strain (ϵ_c) of 1% was induced by a stress of 4.7 ± 0.1 GPa, corresponding to a PBO fiber crystal modulus of about 470 GPa. This can then be used as a calibration for the fiber stress in the model composite. It can be seen in Figure 5a that in the unloaded state the stress is approximately zero along the fiber. (A cold-cured resin was employed so there were very low residual stresses.) As the specimen was loaded, the fiber stress distribution becomes nonuniform and builds up from approximately zero at the fiber end to a plateau value that increases as the load is increased. This behavior is exactly as predicted theoretically from shear-lag analysis[15,16] which forms the basis of composite micromechanics. Similar fiber stress distributions have been obtained in model single-fiber composites using Raman spectroscopy.[17,18] It should be noted that the level of load on the specimen is not stated quantitatively in Figure 5. Since it is possible to determine the local level of stress in the embedded fiber, it is not necessary to know the exact level of external stress or load applied to the specimen.

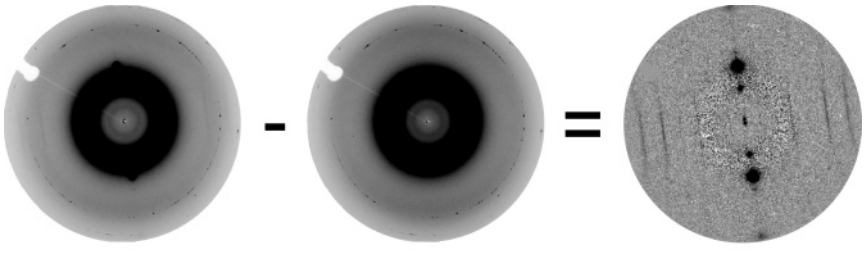

Figure 4. Procedure for subtracting the diffraction pattern of the matrix from that of the fiber and matrix to obtain a diffraction pattern of the fiber only.

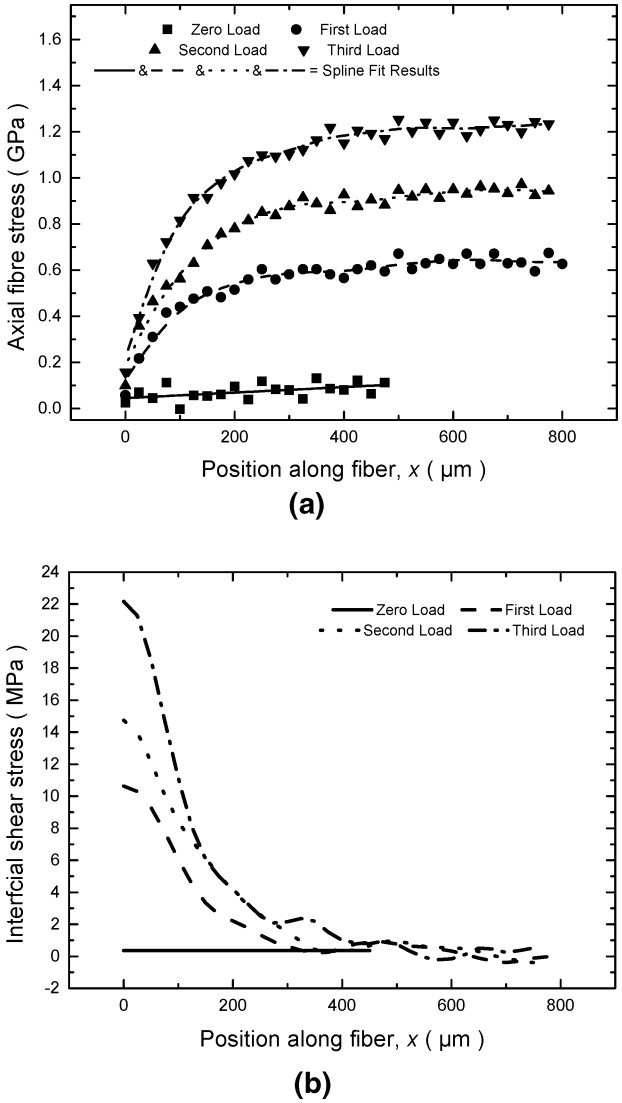

Figure 5. (a) Distributions of axial fiber stress in the PBO/epoxy model composites at different load levels. (b) Derived variations of interfacial shear stress.

It was pointed out earlier that Figures 3 and 4 show that the fiber axis is at about 10° to the specimen tensile axis. It has been demonstrated[19,20] both experimentally and analytically that this leads to the component of strain long the fiber axis being reduced by a factor of $(\cos^2 \theta - \nu \sin^2 \theta)$, where θ is the angle between the fiber axis and tensile axis and ν is the Poisson's ratio of the resin. In this case of $\theta = 10°$ and $\nu \sim 0.35$[20] the axial fiber strain (and therefore stress) will be reduced by no more than 4% of that for an axial fiber with $\theta = 0°$, well within the scatter of the data.

Distributions of fiber stress such those shown in Figure 5a enable the efficiency of stress transfer between the fiber and matrix to be determined. The variation of axial stress, σ_f, along the fiber must be balanced by a shear stress at the fiber/matrix interface. This interfacial shear stress, τ_i, can be determined using an equation based on this force balance[15,16]

$$\tau_i = \frac{r_f}{2}\frac{d\sigma_f}{dx} \tag{4}$$

where r_f is the fiber radius and x is the distance along the fiber. This relationship is generally true for a fiber that is much smaller than the resin surrounding it. However, surface tension at the meniscus of the droplet may change the shear stress profile. Additional terms could be added to the force balance in this case, but this will be assumed to be negligible given that the droplets are large compared to the diameters of the fibers. The variations of interfacial shear stress with x derived from the spline fits to the data in Figure 5a using eq 4 are shown in Figure 5b. It can be seen that τ_i is highest at the fiber ends and then falls in an exponential manner with distance from the fiber end. The overall level of interfacial shear stress increases as the load on the composite increases. The maximum value determined is about 22 MPa, well below the shear yield stress of the resin (~43 MPa[7,18]). It appears that in this case the loading of the composite was not high enough to cause failure of the interface or local yielding the matrix at the fiber ends, as has been observed for similar specimens using Raman spectroscopy.[7,8,18] It is informative to compare the analysis described above with the conventional composite fragmentation test where it is necessary to load the specimen until the fiber undergoes fracture and also to assume a stress distribution in the broken fragments.[16] The use of microfocus X-ray diffraction enables the interfacial shear stress to be determined as a function of position along the fiber at different loading levels without fracturing fibers.

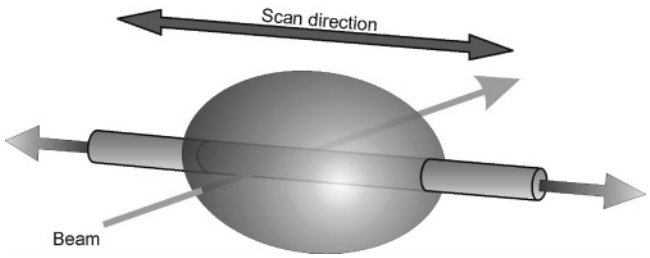

Figure 6. Schematic diagram of the experimental setup for the microdroplet specimen.

Microdroplet Specimens. A schematic diagram of the microdroplet test is shown in Figure 6. This test is different to the geometry used for a traditional composite droplet-debond test[21] in that there is no restraint placed on the droplet to cause detachment. The ability to map the local fiber stress distribution along the fiber inside the droplet at different loading levels means that it is not necessary to measure the force required to detach the droplet from the fiber. The microdroplet specimen was deformed in the deformation rig with a 500 g load cell used previously for the single-fiber deformation studies as described elsewhere.[1] In this case the specimen was aligned in the X-ray beam and then moved incrementally in 20 μm steps through the beam at a number of different fiber stress levels.

The PPTA specimen investigated in this present study had a number of cured epoxy droplets along its length as shown in Figure 7. It can be seen that there are two large droplets of the order of 300−400 μm in diameter and a number of small droplets less than 30 μm in diameter. The bright circular areas in the droplets are artifacts of the illumination system.

Wide-angle X-ray diffraction patterns from the specimen shown in Figure 7 are presented in Figure 8, with the air scattering removed by subtraction using FIT2D. Figure 7a shows a diffraction pattern obtained from a resin-free fiber region. The fiber axis is horizontal, and a well-defined pattern is obtained from the single 12

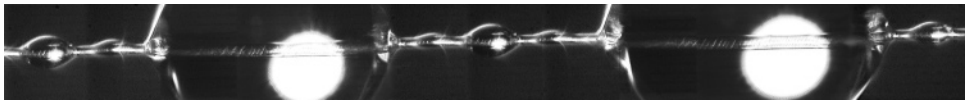

Figure 7. Optical micrograph montage of cured epoxy droplets on a PPTA fiber (diameter of the large droplets: left, 300 μm; right, 400 μm).

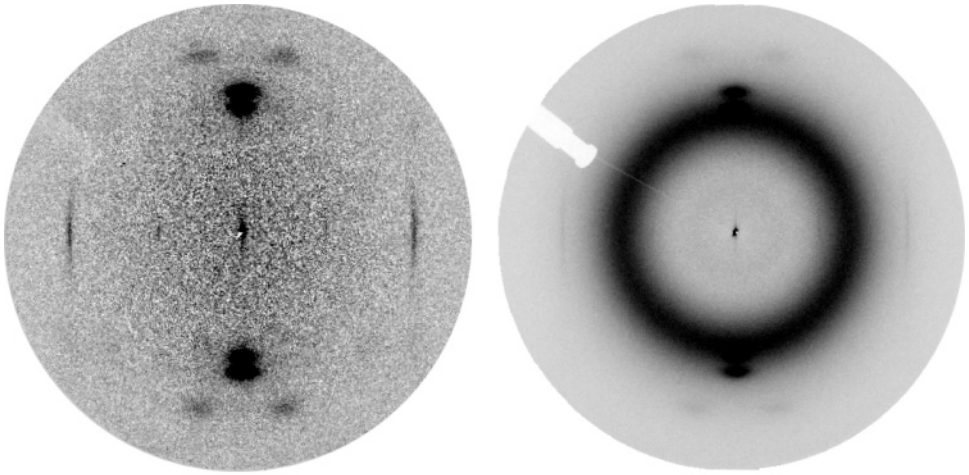

Figure 8. X-ray diffraction patterns from the epoxy microdroplet specimens obtained from (a) outside a droplet and (b) inside a large droplet.

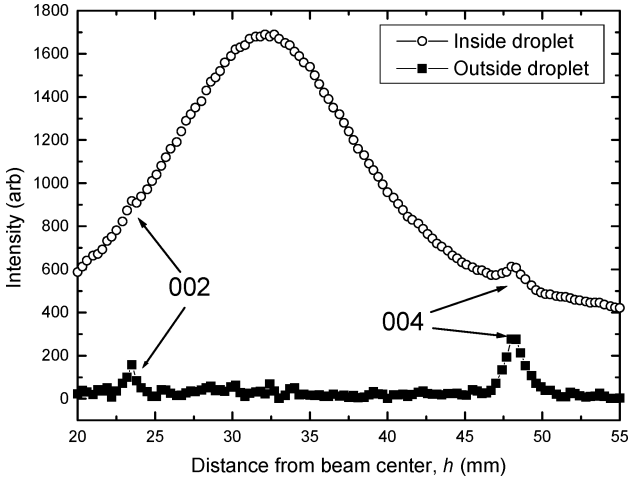

Figure 9. Plots of meridional scattering intensity against distance from the beam center for the diffraction patterns shown in Figure 8.

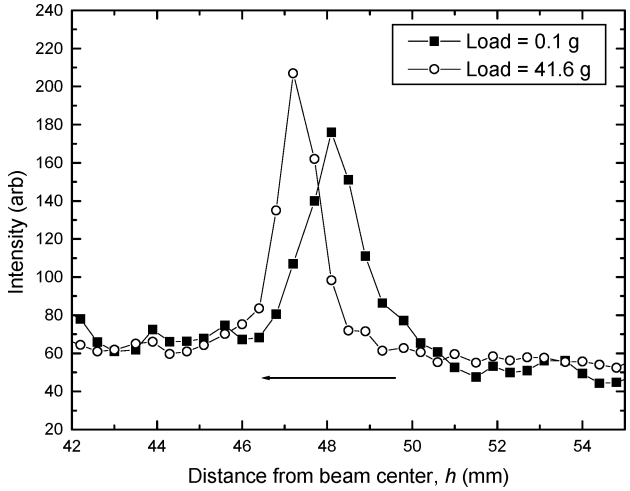

Figure 10. Shift of the 004 peak for the PTTA fiber at the two different indicated load levels.

μm diameter PPTA fiber again with no evidence of radiation damage. A diffraction pattern obtained from the fiber in the center of one of the large droplets is shown in Figure 7b, and it can be seen that it consists of both a ring of amorphous scattering from the resin and a fiber diffraction pattern similar to Figure 7a.

It was possible to obtain an accurate measurement of the positions of the meridional layer lines in the diffraction patterns for the fiber regions both inside and outside the droplet. Figure 9 shows plots of the intensity of scattering along meridional scans with distance from the beam center. The 004 peak of PTTA[22] can be clearly seen in both sets of data whereas the 002 peak is only clear outside the droplet and is obscured by the amorphous halo of the resin inside the droplet.

Well-defined shifts of the meridional peaks were observed when the microdroplet specimens were deformed by subjecting the fibers to tension. This phenomenon is shown in Figure 10 for a PPTA fiber in the undeformed state and at 41.5 g (3.5 GPa). A separate experiment involving the deformation of an individual PPTA fiber showed that these peaks shift linearly by 1% crystal strain (ϵ_c) for a stress of 2.2 ± 0.1 GPa, which corresponds to a crystal modulus of about 220 GPa. This modulus value is similar to that obtained by other workers[23] for the deformation of fiber bundles and calculated theoretically by Rutledge and Suter.[24] Hence, it is possible to determine the local fiber stress from the shift of the 004 peaks under stress.

Failure of the microdroplets specimens was found to take place at stress levels of up to 4 GPa. This is similar to that of a PPTA fiber in air confirming that the microfocus synchrotron radiation did not cause significant radiation damage.

The analysis of the effect of stress upon the microdroplet specimens is shown in Figure 11. As well as being able to determine the point-to-point variation of axial fiber stress, it is also possible to map the geometry of the droplets. Figure 11a shows the variation of the

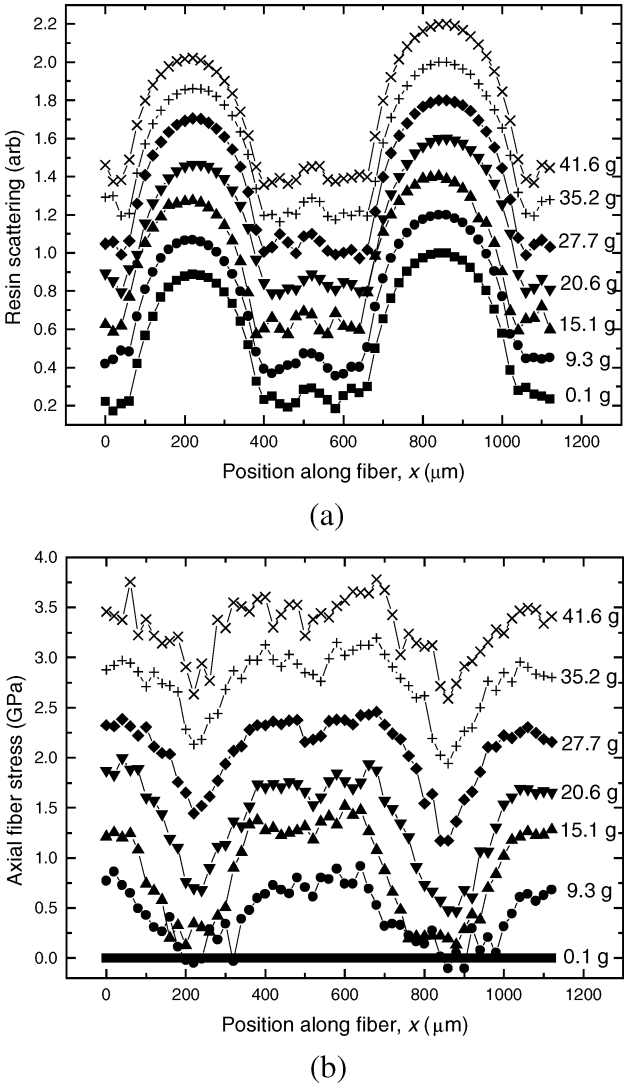

Figure 11. (a) Variation of the intensity of resin scattering and (b) of axial fiber stress with the same position along the fiber for the microdroplet specimen shown in Figure 7.

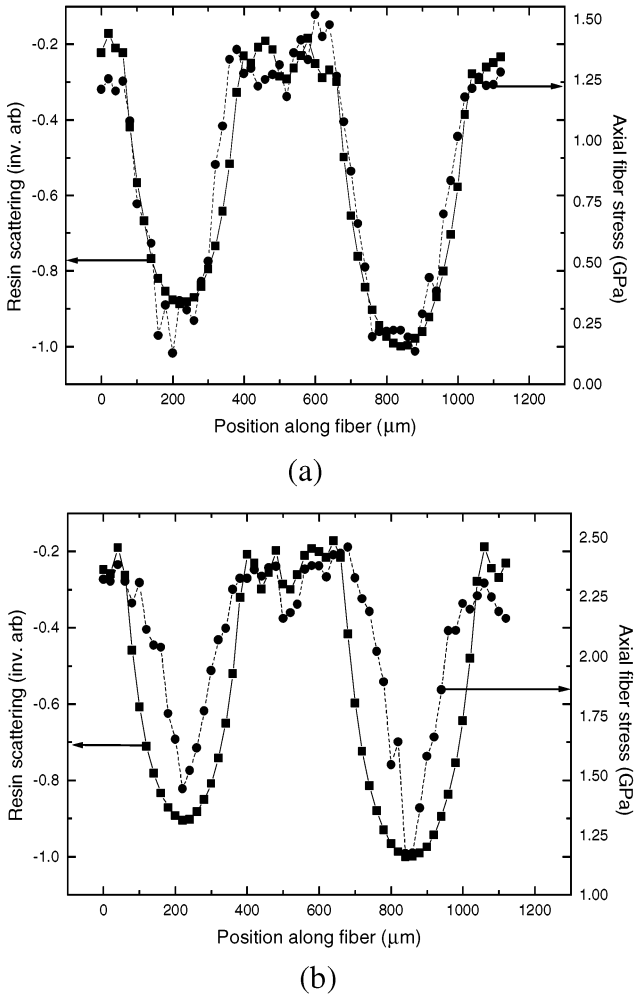

Figure 12. Superimposed plots of the intensity of resin scattering multiplied by (−1) and axial fiber stress at the same position along the fiber for the specimen shown in Figure 7 at loads of (a) 15.1 g and (b) 27.7 g.

total integrated intensity of resin scattering of a Gaussian function fitted to the amorphous halo in a direction at 45° to the fiber axis, with position along the fiber in Figure 7, at different levels of loading. The plots have been normalized to a maximum intensity of unity and are offset for clarity. Since the intensity of scattering will be approximately proportional to the thickness of resin, the plots in Figure 11a are essentially maps of the droplet geometries. It can be seen that they allow an accurate geometry to be determined and that the geometry does not change significantly with fiber loading. It should be pointed out that this approach was only possible because the intensity of the diffraction pattern had been corrected for beam intensity fluctuations using the ionization chamber.

The variation of fiber stress, determined from the shift in the 004 meridional layer line, with position along the fiber (using the same scale as in Figure 11a) at the different loading levels is shown in Figure 11b. It can be seen that the stress outside the droplets increases as the load is increased but that the level of stress in the droplets is less because there is stress transfer from the fiber to matrix within the droplets. The efficiency of this stress transfer depends on the strength of the fiber−matrix interface. It appears that there is interfacial breakdown as the fiber load is increased above about 20 g because the drop in fiber stress in the droplet decreases as the load is increased above this level.

The effect of interfacial breakdown upon the distribution of fiber stress is shown more clearly in Figure 12, which shows the relative distribution of fiber stress and the droplet geometry. The intensity of resin scattering has been multiplied by (−1) and the stress distribution scale adjusted so that the two curves could be superimposed. Figure 12a shows that the two curves can be made to coincide at the lower load. In contrast, when the load on the fiber is increased to 27.7 g, the fiber stress distribution in the droplet becomes triangular, indicating a breakdown of the fiber−matrix interface.[7,8] Equation 4 can again be used to determine the interfacial shear stress in these triangular regions in Figure 12b, and a value of about 30 MPa is obtained for τ_i. In contrast, the slope of the curves of stress with position along the fiber in Figure 12a gave a maximum value of τ_i of 50 MPa, above the shear yield stress of the resin. Hence, it appears that the matrix may have undergone yielding at about 15 g loading and that further deformation leads to a reduced interfacial shear stress due to failure of the interface taking place at higher loading levels.

Higher stress levels can be applied to the interface for the microdroplet specimen than for the embedded

fiber specimen. This is because in the microbond test the stress is transferred from the fiber to matrix, whereas for the fully embedded specimen, stress is transferred from the matrix to fiber. Although the two geometries are somewhat different, since the epoxy matrix is very much weaker than the fiber, matrix fracture will tend to take place at high stresses in fully embedded specimens, limiting the level of stress that can be applied in this geometry.

Conclusions

It has been demonstrated that synchrotron microfocus X-ray diffraction can be used to determine the point-to-point variation of stress in high-performance polymer fibers in an epoxy matrix. The 5 μm diameter is well below the diameter of typical reinforcing polymer fibers and the high-intensity X-ray beam allows diffraction patterns to be obtained with exposure times of only a few seconds without significant radiation damage. Stress-induced shifts in the meridional peaks in the X-ray diffraction patterns have enabled the distribution of fiber stress to be determined in these two-phase systems. The force balance equilibrium allows the shear stress at the fiber−matrix interface to be determined from the fiber stress distribution along the interface.

Although the examples given are for polymer fibers in an epoxy resin matrix, there is considerable scope to extend the technique to the study of deformation micromechanics in other two-phase polymer systems with microstructures on the 10 μm level. For example, the illustrations shown were for a cold-cured epoxy resin where there were no residual stresses. Similar experiments undertaken using hot-cured resin matrices should enable residual stresses to be measured and their effect upon the strength of the fiber−matrix interface to be evaluated. In addition, it should be possible determine fiber stress distributions in model composites with optically opaque matrices, such as polypropylene. Moreover, it may also have extensive applications for other multiphase polymer systems.

Acknowledgment. The authors thank Manfred Burghammer at ID13 for assistance with the experimental configuration and Toyobo and Teijin for supplying fiber samples. Their thanks are also extended to Andrew Hammersley for use of the FIT2D software application and colleagues in the Manchester Materials Science Centre who have collaborated in this study.

References and Notes

(1) Davies, R. J.; Montes-Morán, M. A.; Riekel, C.; Young, R. J. *J. Mater. Sci.* **2001**, *36*, 3079.
(2) Montes-Morán, M. A.; Davies, R. J.; Riekel, C.; Young, R. J. *Polymer* **2002**, *43*, 5219.
(3) Davies, R. J.; Montes-Morán, M. A.; Riekel, C.; Young, R. J. *J. Mater. Sci.* **2003**, *38*, 2105.
(4) Yang, H. H. *Kevlar Aramid Fiber*; John Wiley & Sons: New York, 1993.
(5) Beers, D.; Young, R. J.; So, C. L.; Sikkema, D. J.; Perepelkin, K. E.; Weedon, G. *High Performance Fibres*; Hearle, J. W. S., Ed.; Woodhead Publishing Ltd.: Cambridge, UK, 2001; p 93.
(6) Kitagawa, T.; Murase, H.; Yabuki, K. *J. Polym. Sci., Polym. Phys.* **1998**, *36*, 39.
(7) So, C.-L.; Young, R. J. *Plast. Rubber Comp., Proc. Appl.* **1997**, *26*, 423.
(8) Bennett, J. A.; Young, R. J. *Comp. A: Appl. Sci. Manufact.* **1998**, *29*, 1071.
(9) de Lange, P. J.; Mäder, E.; Mai, K.; Young, R. J.; Ahmad, I. *Comp. A: Appl. Sci. Manufact.* **2001**, *32*, 331.
(10) Eichhorn, S. J.; Young, R. J. *Compos. Sci. Technol.* **2004**, *64*, 767.
(11) Hammersley, A. P.; Riekel, C. MFIT: Multiple Spectra Fitting Program. *Synch. Rad. News* **1989**, *2*, 24.
(12) Hammersley, A. P. FIT2D: An Introduction and Overview. ESRF Int. Rep., ESRF97HA02T, 1997.
(13) Young, R. J.; Lovell, P. A. *Introductions to Polymers*, 2nd ed.; Chapman & Hall: London, 1992.
(14) Kozey, V. V.; Jiang, H.; Mehta, V. R.; Kumar, S. *J. Mater. Res.* **1995**, *10*, 1044.
(15) Kelly, A.; MacMillan, N. H. *Strong Solids*, 3rd ed.; Clarendon Press: Oxford, 1980.
(16) Piggott, M. R. *Load Bearing Fibre Composites*; Pergamon Press: Oxford, UK, 1980.
(17) Young, R. J.; Galiotis, C.; Robinson, I. M.; Batchelder, D. N. *J. Mater. Sci.* **1987**, *22*, 3642.
(18) Andrews, M. C.; Young, R. J. *J. Raman Spectrosc.* **1993**, *24*, 539.
(19) Fan, C. F.; Hsu, S. L. *J. Polym. Sci., Part B: Polym. Phys.* **1989**, *27*, 2605.
(20) Day, R. J.; Hu, X.; Young, R. J. *J. Mater. Sci., Lett.* **1992**, *11*, 1344.
(21) Chou, C. T.; Gaur, U.; Miller, B. *Compos. Sci. Technol.* **1994**, *51*, 111.
(22) Riekel, C.; Cedola, A.; Heidelbach, F.; Wagner, K. *Macromolecules* **1997**, *30*, 1033.
(23) Gaymans, R. J.; Tijssen, J.; Harkema, S.; Bantjes, A. *Polymer* **1976**, *17*, 517.
(24) Rutledge, G. C.; Suter, U. W. *Polymer* **1991**, *32*, 2179.

MA048484X